SUBHARMONIC ELECTROMAGNETIC RADIATION FROM CAVITONS

T. Tanikawa and A. Y. Wong

In a high-power microwave-plasma system, it has been experimentally found that electromagnetic (em) radiation at subharmonic frequencies [specifically, $(3/2)\omega_0$ and $(5/2)\omega_0$] of the electron plasma frequency of the unperturbed state, ω_0, can be emanated from cavitons which are resonantly driven by an intense em pulse (frequency ω_0) in an unmagnetized inhomogeneous plasma. Electron oscillations at $\sim (1/2)\omega_0$ are preferentially excited inside a deep ($|\delta n/n_c| \geq 0.5$) caviton although this is not deep enough to resonantly support $(1/2)\omega_0$ oscillations. The experimental results show that the coupling between the $(1/2)\omega_0$ electron oscillations inside the caviton and the electron plasma waves at ω_0, which is originally excited due to the mode conversion of the incident microwave at the resonant layer and which generates the caviton, produces a localized nonlinear current which emits em waves at $(3/2)\omega_0$. A similar coupling between $(3/2)\omega_0$ and ω_0 frequencies can emit em waves at $(5/2)\omega_0$. The model to explain the above new phenomenon is discussed.

1. INTRODUCTION

When plasma interact with intense electromagnetic (em) waves frequency ω_0, emissions at $n\omega_0$ (where, $n = 2, 3, \ldots$) as well as at $(n' + 1/2)\omega_0$ (where, $n' = 0, 1, 2, \ldots$) can be generated due to various nonlinear processes. For instance, emissions at harmonic and subharmonic frequencies of the incident em wave frequency have been observed during ionospheric modification experiments [1].

In laser-plasma interaction experiments, the scattered light at frequencies different from the frequency ω_0 of the incident laser light is considered to be useful for the diagnosis of coronal plasmas. For example, the scattered light at $(3/2)\omega_0$ is often used to locate the quarter-critical layer, where the local plasma density is equal to one-quarter of the critical density n_c defined by $n_c \equiv m\omega_0^2/(4\pi e^2)$, since it is attributed to the result of the two-plasmon ($2\omega_p$) decay instability at that layer [2, 3]. The spectral characteristics of $(1/2)\omega_0$ emission have been used to determine the coronal electron temperature [4]. The filanentation instability has been identified through the simultaneous measurements of $(3/2)\omega_0$, $2\omega_0$ and x-ray emissions [5].

In this paper, we wish to present the experimental evidence of the new generation mechanism of $(3/2)\omega_0$ em radiation from an unmagnetized inhomogeneous plasma which is exposed to an intense em wave of frequency ω_0. The generation mechanism of $(3/2)\omega_0$ radiation is usually considered to be the scattering of the incident em wave at ω_0 by the electron plasma waves

(EPWs) at $(1/2)\omega_0$ generated by the $2\omega_p$ decay instability at the $(1/4)n_c$ layer; hence, $(3/2)\omega_0$ radiation can be used to identify that layer. However, our experimental results show that $(3/2)\omega_0$ em radiation can also be generated at the critical layer, where the local electron plasma frequency in the unperturbed state matches the frequency of the incident em wave, ω_0, when deep density cavities (or cavitons) are generated at this layer by irradiating an inhomogeneous plasma with an intense em wave. We, therefore, note here that the possible pitfall of the common practice in which $(3/2)\omega_0$ radiation is used to diagnose underdense plasmas near $(1/4)n_c$ because $(3/2)\omega_0$ radiation can originate from cavitons generated near n_c.

Cavitons are localized EPWs trapped inside density cavities which are generated by ponderomotive forces associated with the localized waves themselves [6]. In our experiment, a high-power microwave beam is injected into an unmagnetized inhomogeneous plasma. Intense localized EPWs of frequency ω_0 are resonantly excited at the critical layer; they evolve to cavitons and the EPWs at ω_0 are trapped inside the deep density cavities. The trapped wave in a caviton undergoes a parametric type decay process inside the cavity, enhancing electron oscillations at $(1/2)\omega_0$ when the cavity is sufficiently deep ($|\delta n/n_c| \geq 0.5$). If the intensity of the initially excited EPW at ω_0 in the caviton exceeds a certain threshold determined by the depth and shape of the cavity, the amplitude of the $(1/2)\omega_0$ oscillations inside the caviton can grow even if they are not the eigenmode of the caviton. The coupling between the $(1/2)\omega_0$ electron oscillations and the "pump" EPW at ω_0 produces a localized nonlinear current which emits em waves at $(3/2)\omega_0$. A similar process can further produce em waves at $(5/2)\omega_0$, *etc.* We have experimentally observed up to $(5/2)\omega_0$ subharmonic emissions. Detailed discussions regarding the physical processes leading to the generation of subharmonic emissions. Detailed discussions regarding the physical processes leading to the generation of subharmonic em radiation are given in Sections 4 and 5.

First, the experimental apparatus and the diagnostic techniques employed in our work are described in Section 2. The experimental observations are then reviewed in Section 3. In Section 4, a possible mechanism of preferentially enhancing $(1/2)\omega_0$ electron oscillations in cavitons is described, and in Section 5, the emission power of $(3/2)\omega_0$ radiation is estimated. Finally, Section 6 is the concluding summary.

2. EXPERIMENTAL SETUP

Our experiment was performed in a high-power microwave-plasma system which consists of a large ($\sim$ 1.4 m diameter, $\sim$ 2.3 m length) vacuum vessel (see Fig. 1) [7]. A plasma is produced using a pulsed, high-power hf transmitter ($f_{hf} \approx 400$ kHz, $P_{max} \approx 15$ kW) connected to a discharge loop antenna ($\sim$ 80 cm diameter) located near one end of the chamber. With the maximum

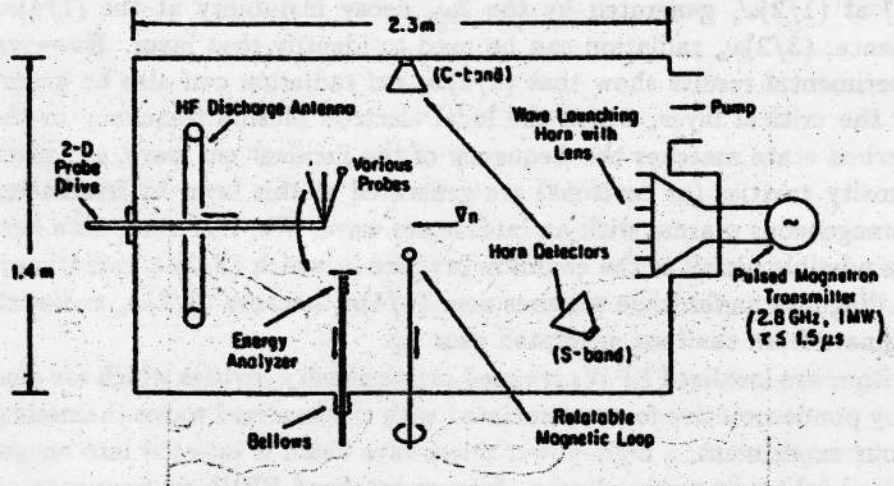

Fig.1. Schematic diagram of the experimental apparatus.

transmitter power of nearly 15 kW, plasma density of $n \sim 3 \times 10^{11}$ cm^{-3} can be obtained for argon (Ar) gas with the neutral pressure of $p_n \approx 3 \times 10^{-4}$ Torr. The experiment was performed in a quiescent ($|\delta n/n| < 0.3\%$) afterglow plasma. Since the plasma is mainly produced at one end of the chamber near the discharge loop antenna and flows with approximately the ion acoustic speed, a density gradient is naturally created along the axis of the chamber. A desired density–gradient scale–length, $L \equiv n_e(\partial n/\partial z)^{-1}$, can be obtained by adjusting the discharge transmitter power and by selecting a proper afterglow time to carry out measurements, where z is the axial position. Typical plasma parameters for an Ar plasma are: $n \approx 1 \times 10^{11}$ cm^{-3}, $T_e \approx 6T_i \approx 1.5$ eV, $\lambda_D \approx 3 \times 10^{-3}$ cm, $L = 50 \sim 100$ cm $= (1.7 \sim 3.5) \times 10^4 \lambda_D$, $p_n \approx 3 \times 10^{-4}$ Torr and $\nu_{en}/\omega_{pe} \approx 4 \times 10^{-4}$. Our microwave source is a pulsed, high–power ($P_{in} \leq 500$ kW) magnetron operated at $f_0 = \omega_0/2\pi = 2.815$ GHz. The pulse duration can be adjusted between 0.15 μs and 1.2 μs. The microwave is launched from the horn antenna with a focusing lens mounted at the low–density end of the plasma column. This system can provide the microwave intensity of up to $|\tilde{E}_0|^2/(8\pi n_e T_e) = 0.5$, where $\tilde{E}_0$ is the amplitude of the vacuum electric field associated with the incident microwave.

Subharmonic em radiation was detected by using a C-band horn antenna mounted outside the plasma column so as not to disturb the sensitive interaction region. When the measurements were carried out, all probe structures were moved to the outside of the plasma column to ensure that they would not produce spurious signals especially near $(3/2)\omega_0$ due to nonlinear probe effects, such as the sheath–plasma instability [8, 9]. Before feeding the signal into the detection circuitry, a long ($\sim$ 2 m) C-band waveguide was used as a high–pass filter in order to eliminate an intense signal at the fundamental frequency ω_0 which was capable of producing spurious signals in the detection system.

Since electron oscillations at $(1/2)\omega_0$ were generated in cavitons surrounded by an overdense plasma in which waves at $(1/2)\omega_0$ were evanescent, it was not possible to detect signals at $(1/2)\omega_0$ by antennas located outside the plasma column. Therefore, we decided to insert a small, electrostatically insulated antenna to pick up the signals at $(1/2)\omega_0$ with a minimal disturbance to the sensitive interaction region. Other measurements confirmed that this disturbance was in fact negligible.

In order to measure basic plasma parameters, such as the plasma density, the electron temperature and the plasma space potential, plane ($\sim$ 1 mm diameter) and cylindrical ($\sim$ 0.25 mm diameter, $\sim$ 5 mm length) Langmuir probes were used in a usual manner. In most cases, the measurements were carried out just after the termination of the incident microwave pulse using a box–car integrator in order to avoid nonlinear probe effects due to strong rf fields [8, 9].

3. EXPERIMENTAL RESULTS

We have detected $(3/2)\omega_0$ em radiation by the C-band horn antenna shown in Fig.1 when the critical layer exists in the spatial region that is covered by the main lobe of the horn antenna. We have confirmed that this $(3/2)\omega_0$ radiation originates from the cavitons generated at the critical layer. Although we have observed $(3/2)\omega_0$ em radiation when the $(1/4)n_c$ layer exists in the central region of the plasma column as well, we will concentrate on the discussion of the $(3/2)\omega_0$ radiation from cavitons at the critical layer since the purpose of this paper is to describe the new generation mechanism of subharmonic emissions from a plasma under strong em irradiation. We note here that the $(3/2)\omega_0$ radiation observed in the underdense plasma can be attributed to the $2\omega_p$ decay instability near the $(1/4)n_c$ layer because the intensity of our microwave beam always exceeds the threshold intensity for the $2\omega_p$ decay instability under our experimental conditions.

In our experiment, the cavitons are generated as blobs of low density regions on the critical surface as shown in Fig.2(a). The unperturbed density profile is also shown in Fig.2(b) for comparison. The depth of the central caviton at $r = 0$ cm and $z = 41.5$ cm is approximately 55% of the critical density. This caviton is sufficiently deep to cause electron oscillations at $(1/2)\omega_0$ enhanced, as discussed in Section 4. The cut–out density profile along the axis of the plasma column, *i.e.*, along the $r = 0$ line, is shown in Fig.2(c).

Since waves at $(1/2)\omega_0$ are evanescent in the plasma region surrounding the cavitons, $(1/2)\omega_0$ signals cannot be detected using antennas situated outside the plasma column even if $(1/2)\omega_0$ electron oscillations exist in the cavitons. In order to detect signals at $(1/2)\omega_0$, a small electrostatically insulated antenna to detect either oscillating electric or magnetic fields was inserted into the critical region. Figure 3 shows the intensity of the $(1/2)\omega_0$ signal detected by

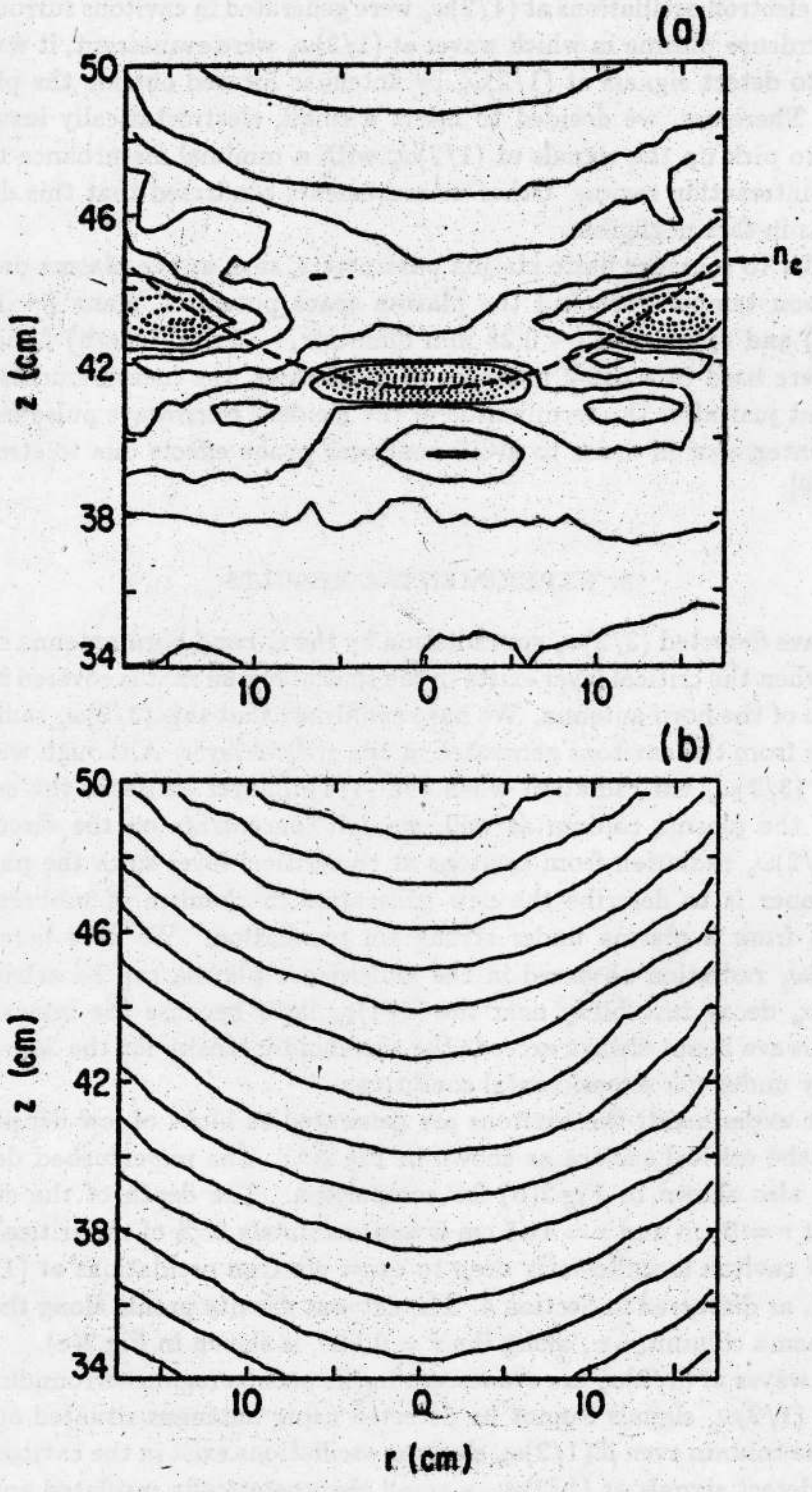

Fig.2(a) and Fig.2(b)

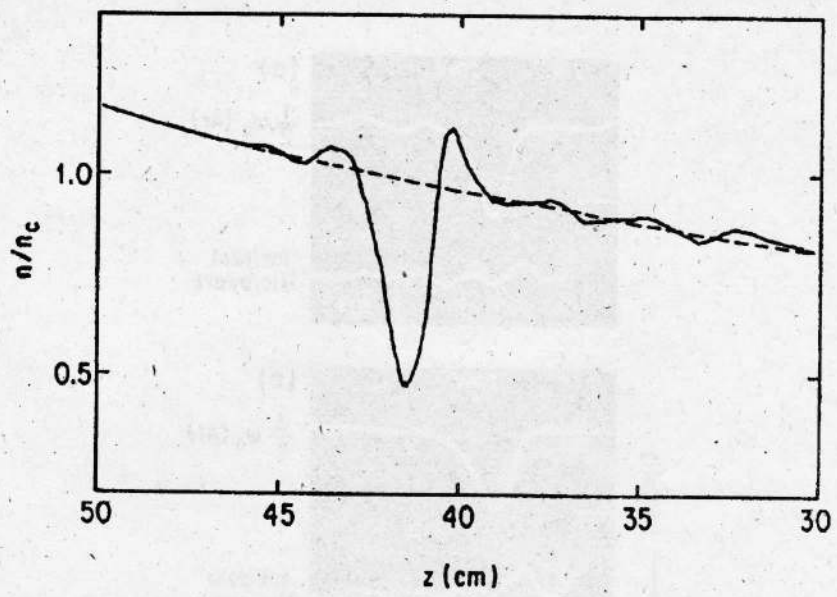

Fig.2. Development of a three–dimensional structure in cavitons.
a) Density profile after injecting a short ($\Delta t_{rf} \sim 0.15\mu s$) microwave pulse of $P_{in} \sim 200$ kW. The deep density cavities are indicated by the dashed contour lines. The initial critical surface is indicated by the thick dashed curve. The increment between adjacent contour lines is 5.7% of the critical density n_c.
b) Density profile just before the injection of the microwave pulse. The axial density–gradient scale–length L is 60 cm. The increment between adjacent contour lines is 2.5% of the critical density n_c.
c) Perturbed density profile along the axis of the plasma column (*i.e.*, at $r = 0$ cm). The deep density cavity ($|\delta n/n_c| \approx 0.55$) corresponds to the central low density "blob" on the contour map.

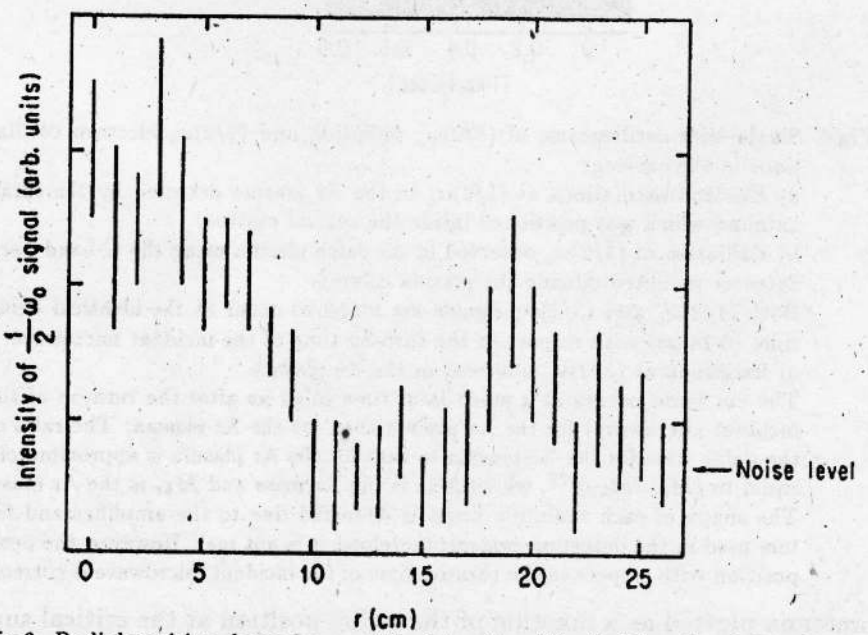

Fig.3. Radial position dependence of the intensity of the $(1/2)\omega_0$ signal detected by a small, electrostatically insulated antenna.

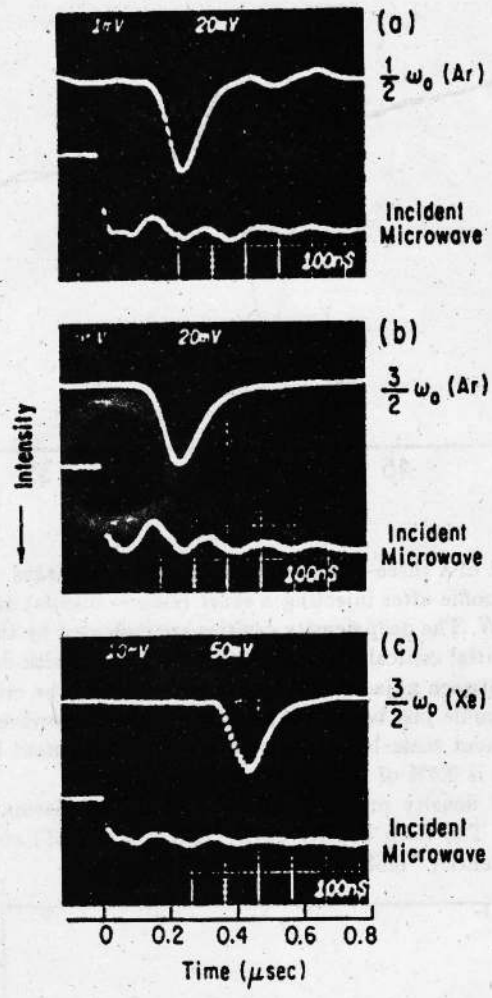

Fig.4. Single–shot oscillograms of $(3/2)\omega_0$ radiation and $(1/2)\omega_0$ electron oscillations in the caviton.
a) Electron oscillations at $(1/2)\omega_0$ in the Ar plasma detected by the small antenna which was positioned inside the central caviton.
b) Radiation at $(3/2)\omega_0$ observed in the same plasma using the C-band horn detector mounted outside the plasma column.
Both $(1/2)\omega_0$ and $(3/2)\omega_0$ signals are found to occur at the identical delay time (0.24 μs) with respect to the turn-on time of the incident microwave.
c) Radiation at $(3/2)\omega_0$ observed in the Xe plasma.
The em burst occurs at a much later time (0.43 μs after the turn-on of the incident microwave) for the Xe plasma than for the Ar plasma. The ratio of the delay time for the Xe plasma to that for the Ar plasma is approximately equal to $(M_{Xe}/M_{Ar})^{1/2}$, where M_{Xe} is the Xe mass and M_{Ar} is the Ar mass. The shape of each radiation burst is distorted due to the amplifier and filters used in the detection system; therefore, it is not real. However, the peak position with respect to the turn-on time of the incident microwave is correct.

the antenna plotted as a function of the radial position at the critical surface. Peaks are observed in the intensity of the $(1/2)\omega_0$ signal when the antenna

passes the central and outer cavitons. This result is clear evidence that $(1/2)\omega_0$ electron oscillations are, in fact, generated inside the cavitons of $|\delta n/n_c| \geq 0.5$.

As shown in Fig.4, the radiation at $(3/2)\omega_0$ and the $(1/2)\omega_0$ electron oscillations are generated as short bursts. The duration of each burst is typically 0.13 μs (FWHM). As can be seen from Figs. 4(a) and 4(b), the coincidence between the $(1/2)\omega_0$ and $(3/2)\omega_0$ signals is evidence that the generation of $(3/2)\omega_0$ radiation directly correlates to that of $(1/2)\omega_0$ electron oscillations in cavitons. The occurrence time of the radiation burst roughly coincides with the time of caviton formation ($\sim 16\omega_{pi}^{-1}$); therefore, it accordingly increases for the Xe plasma by the factor of $(M_{Xe}/M_{Ar})^{1/2}$ as seen in Fig.4(c), where M_{Xe} and M_{Ar} are the Xe mass and the Ar mass, respectively.

The power of $(3/2)\omega_0$ radiation collected by the C-band horn antenna increases linearly with the incident microwave power as shown in Fig.5. Since

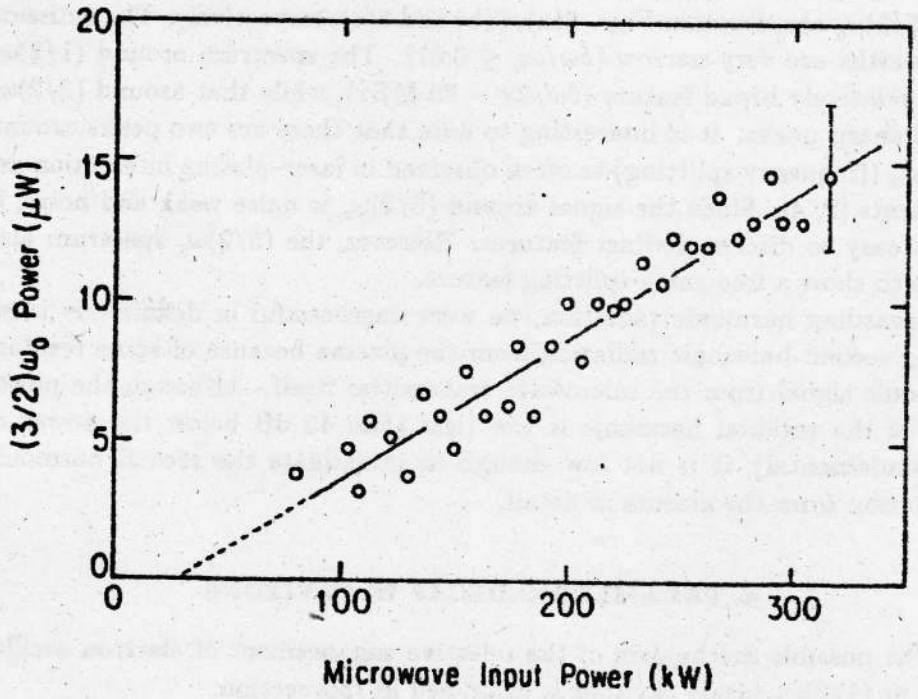

Fig.5. Power of the $(3/2)\omega_0$ radiation collected by the C-band horn detector versus the input microwave power, P_{in}. The straight line is a least-square fit for the data points.

the depths of density cavities tend to saturate after the input microwave power exceeds a certain level, the depth of each cavity is nearly constant ($|\delta n/n_c| = 0.53 \sim 0.6$) over the range of input microwave power used in our experiment. Therefore, it is expected that the conversion efficiency from the resonantly excited EPW at ω_0 to $(1/2)\omega_0$ electron oscillations and eventually to $(3/2)\omega_0$ em waves in each caviton is also nearly constant (see Sections 4 and 5). The

role of the incident microwave power is then to increase the intensity of the ω_0 EPW accordingly, leading to the linear increase in the power radiated at $(3/2)\omega_0$ with the input microwave power. The collected power of $(3/2)\omega_0$ radiation is approximately 100 dB lower than the input microwave power. Extrapolation of the data seems to indicate the existence of the threshold input microwave power of $\sim$ 25 kW or higher for the generation of $(3/2)\omega_0$ radiation. Because our magnetron microwave source cannot be operated below the power level of $\sim$ 80 kW, the exact threshold input power has not yet been determined.

In our experiment, subharmonic em radiation up to $(5/2)\omega_0$ has been observed. Frequencies higher than $(5/2)\omega_0$ cannot be detected due to instrumental limitation. Although the single–shot behaviors of various subharmonics are closely related to one another (in fact, their appearances coincide with one another), their power spectra show different features. The time integrated frequency spectra of $(1/2)\omega_0$ electron oscillations and em radiation at $(3/2)\omega_0$ and $(5/2)\omega_0$ are shown in Figs. 6(a), 6(b) and 6(c), respectively. The emission bandwidths are very narrow ($\delta\omega/\omega_0 \leq 0.01$). The spectrum around $(1/2)\omega_0$ has a relatively broad feature ($\delta\omega/2\pi \sim 30$ MHz), while that around $(3/2)\omega_0$ shows sharp peaks. It is interesting to note that there are two peaks around $(3/2)\omega_0$ (frequency splitting) as often observed in laser–plasma interaction experiments [2, 4]. Since the signal around $(5/2)\omega_0$ is quite weak and noisy, it is not easy to discern distinct features. However, the $(5/2)\omega_0$ spectrum also seems to show a frequency splitting feature.

Regarding harmonic radiation, we were unsuccessful in definitively identifying second harmonic radiation from the plasma because of some residual harmonic signal from the microwave transmitter itself. Although the power level of the residual harmonic is low (less than 40 dB below the power of the fundamental), it is not low enough to investigate the second harmonic generation from the plasma in detail.

4. PARAMETRIC DECAY IN CAVITONS

The possible mechanism of the selective enhancement of electron oscillations at $(1/2)\omega_0$ inside cavitons is examined in this section.

Our experimental results show that the depth of the cavitons created at the critical density n_c. However, cavitons of $|\delta n/n_c| \geq 0.75$, in which the plasma density at the bottom of a cavity $n_B \leq (1/4)n_c$, have never been observed in our experiment. Even so, electron oscillations at very close to $(1/2)\omega_0$ are observed to be preferentially enhanced in the cavitons. We shall see that this is possible because a deep caviton acts as a parametrically driven harmonic oscillator. Here, the EPW at frequency ω_0 trapped in the caviton plays a role of a "pump". The lowest ($\ell = 0$) and the second-lowest ($\ell = 1$) caviton eigenmodes [6] (a "signal" and an "idler") can then couple with each other

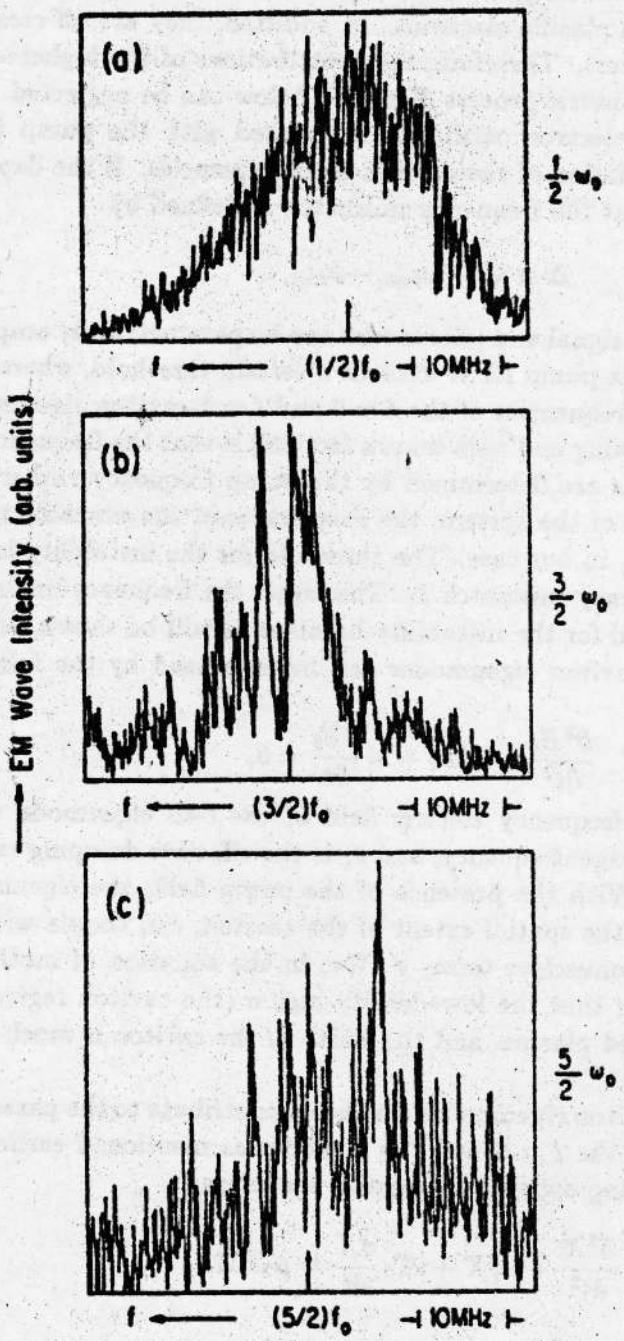

Fig.6. Frequency spectra of the subharmonic radiation from the caviton. Frequency spectra around (a) $(1/2)\omega_0$, (b) $(3/2)\omega_0$, and (c) $(5/2)\omega_0$ are presented. The frequency increases toward the left-hand side along the abscissa. The ordinate (intensity) is indicated in a linear scale. The experimental conditions are $\Delta t_{rf} \sim 1.2\mu s$ and $P_{in} \sim 290$ kW.

through this pump [10]. The higher–order eigenmodes are heavily damped because their effective wavelengths in the caviton are short, resulting in the strong interactions with plasma electrons. In addition, they are off-resonant for this parametric process. Therefore, the contributions of the higher–order eigenmodes to the parametric process discussed below can be neglected.

A large–amplitude electron oscillation associated with the pump EPW causes a periodic modulation of the caviton eigenfrequencies. If the depth of the cavity is so deep that the frequency mismatch Δ defined by

$$\Delta \equiv \omega_0 - \omega_{\ell=0} - \omega_{\ell=1} \tag{1}$$

is sufficiently small, the signal and idler modes can be parametrically amplified when the intensity of the pump EPW exceeds a certain threshold, where $\omega_{\ell=0}$ and $\omega_{\ell=1}$ are the eigenfrequencies of the $\ell = 0$ and $\ell = 1$ caviton eigenmodes, respectively. An interesting and well–known fact [10] is that the frequencies of the unstable oscillations are determined by the pump frequency rather than the natural frequencies of the system; the frequencies of the unstable modes are "locked" at $(1/2)\omega_0$ in our case. The threshold for the instability is then a function of the frequency mismatch Δ. The larger the frequency mismatch, the higher the threshold for the instability becomes as will be shown below.

The evolution of caviton eigenmodes can be expressed by the following equation:

$$\frac{\partial^2 E_\ell}{\partial t^2} + \omega_\ell^2 E_\ell + \nu_\ell \frac{\partial E_\ell}{\partial t} = 0, \tag{2}$$

where E_ℓ is the high–frequency electric field of the ℓ-th eigenmode of the caviton, ω_ℓ is the ℓ-th eigenfrequency, and ν_ℓ is the effective damping rate for the ℓ-th eigenmode. With the presence of the pump field, the eigenmodes, which are localized in the spatial extent of the caviton, can couple with one another through the convective term, $\mathbf{v} \cdot \nabla \mathbf{v}$, in the equation of motion for the electrons. We note that the low–density region (the caviton region) can be treated as a bounded plasma, and the width of the caviton is much larger than the Debye length.

In our case, the caviton eigenmodes which can contribute to the parametric instability process are the $\ell = 0$ and $\ell = 1$ modes as mentioned earlier. We then obtain the following coupled differential equations:

$$\frac{\mathrm{d}^2 X}{\mathrm{d}t^2} + \omega_1^2 X + 2\Gamma_1 \frac{\mathrm{d}X}{\mathrm{d}t} = \mu_2 Y Z, \tag{3a}$$

$$\frac{\mathrm{d}^2 Y}{\mathrm{d}t^2} + \omega_2^2 Y + 2\Gamma_2 \frac{\mathrm{d}Y}{\mathrm{d}t} = \mu_1 X Z, \tag{3b}$$

where

$$\omega_1 \equiv \omega_{\ell=0}, \qquad \omega_2 \equiv \omega_{\ell=1},$$

$$X(t) \equiv E_{\ell=0}(t), \qquad Y(t) \equiv E_{\ell=1}(t), \tag{4}$$
$$\Gamma_1 \equiv \nu_{\ell=0}/2, \qquad \Gamma_2 \equiv \nu_{\ell=1}/2.$$

The pump EPW at frequency ω_0 is represented by

$$Z \equiv 2Z_0 \cos(\omega_0 t) = \tilde{E}_0 \cos(\omega_0 t), \tag{5}$$

and the coupling coefficients for the coupling of the pump EPW with the $\ell = 0$ and $\ell = 1$ modes are denoted by μ_1 and μ_2, respectively.

Fourier transformation of the set of equations (3) gives

$$D_1(\omega)X(\omega) + \mu_2 Z_0[Y(\omega - \omega_0) + Y(\omega + \omega_0)] = 0, \tag{6a}$$

$$D_2(\omega)Y(\omega) + \mu_1 Z_0[X(\omega - \omega_0) + X(\omega + \omega_0)] = 0, \tag{6b}$$

where

$$D_1(\omega) \equiv \omega^2 + 2i\Gamma_1\omega - \omega_1^2, \tag{7a}$$

$$D_2(\omega) \equiv \omega^2 + 2i\Gamma_2\omega - \omega_2^2. \tag{7b}$$

Since we seek for the solution to Eqs. (6a) and (6b) around $\omega \sim \omega_1$, with the conditions $\omega_0 \sim 2\omega_1$ and $\omega_1 \sim \omega_2$, the frequency $\omega + \omega_0$ is off-resonant. Therefore, Eqs. (6a) and (6b) can be reduced to

$$D_1(\omega)X(\omega) + \mu_2 Z_0 Y(\omega - \omega_0) = 0, \tag{8a}$$

$$\mu_1 Z_0 X(\omega) + D_2(\omega - \omega_0)Y(\omega - \omega_0) = 0. \tag{8b}$$

In order for these equations to have a nontrivial solution, the following nonlinear dispersion relation has to be satisfied:

$$D_1(\omega)D_2(\omega - \omega_0) = \mu_1\mu_2 Z_0^2. \tag{9}$$

Using $\Delta \equiv \omega_0 - \omega_1 - \omega_2$ and $\xi \equiv \omega - \omega_1$, Eq. (9) can be rewritten as

$$2\omega_1(\xi + i\Gamma_1)[-2\omega_2(\xi - \Delta + i\Gamma_2)] = \mu_1\mu_2 Z_0^2, \tag{10}$$

where we have used $|\xi - \Delta| \ll 1$. Writing $\xi = x + iy$, the real and imaginary parts of Eq. (10) give

$$(x^2 - y^2) - \Delta x - (\Gamma_1 + \Gamma_2)y + \Xi^2/4 - \Gamma_1\Gamma_2 = 0 \tag{11}$$

and

$$2xy + (\Gamma_1 + \Gamma_2)x - \Delta y - \Gamma_1\Delta = 0, \tag{12}$$

where

$$\Xi^2 \equiv \frac{\mu_1 \mu_2 Z_0^2}{\omega_1 \omega_2}. \tag{13}$$

Noting the fact that $y = 0$ at the threshold for the parametric instability and assuming $\Gamma_1 \sim \Gamma_2$, we can solve Eqs. (11) and (12) to obtain the following condition for the decay instability in the caviton:

$$\Xi^2 \geq \Delta^2 + 4\Gamma_1\Gamma_2. \tag{14}$$

At the threshold given by Eq. (14), we have $x = \Delta/2$ which yields the frequency of the decayed mode:

$$\mathrm{Re}(\omega) = \frac{1}{2}\omega_0 \pm \frac{1}{2}(\omega_1 - \omega_2). \tag{15}$$

Substituting $x = \Delta/2$ into Eq. (11) and solving the resultant equation for y, we obtain the growth rate of the decayed mode:

$$\gamma = y \simeq \frac{1}{2}[(\Xi^2 - \Delta^2)^{1/2} - (\Gamma_1 + \Gamma_2)]. \tag{16}$$

In Eq. (15), either a plus or a minus sign can be selected depending upon which mode ($\ell = 0$ or $\ell = 1$) is dominant in the real situation.

According to Tanikawa *et al.* [6], the $\ell = 0$ mode has a spatial profile which is symmetric around the center of the caviton, while the $\ell = 1$ mode has a profile which is antisymmetric around the same point. This leads us to expect that μ_2 is much smaller than μ_1 since the spatial overlapping of the $\ell = 1$ mode with the pump EPW tends to cancel out the effect of the coupling [11]. Therefore, we expect that the degenerate parametric process, in which both of the decayed modes are the $\ell = 0$ mode, is the dominant process in our case. For the degenerate case, the coupling coefficient can be represented by [12]

$$|\mu_1| = |\mu_2| \simeq 2\pi \frac{e}{m} \frac{1}{W}, \tag{17}$$

where W is the width of the caviton. Using Eqs. (13), (14) and (17), the threshold field strength of the pump EPW at ω_0 for the degenerate parametric process is given by

$$|\tilde{E}_0|_{\mathrm{th}} \simeq \left(\frac{m}{\pi e}\right) \omega_1 W[(\Delta^2 + \nu_1^2)]^{1/2}. \tag{18}$$

From Eq. (15), we can see that the frequency of the unstable mode for the degenerate case exactly equals one-half of the incident microwave frequency since $\omega_1 = \omega_2$.

We now estimate the threshold field strength of the pump EPW at ω_0 for the parametric enhancement of $(1/2)\omega_0$ electron oscillations inside the cavitons

observed in our experiment. The spatial overlapping or phase relationship between the pump EPW and the $\ell = 0$ mode is the most favorable among the couplings between the different caviton eigenmodes through the pump EPW at ω_0; as a result, the threshold for the degenerate parametric process is the lowest [see Eq. (14)]. For this reason, we consider the degenerate case below. Here, we use Eq. (14) in Tanikawa *et al.* [6] to estimate the caviton eigenfrequencies. A typical caviton observed in our experiment is pancake–shaped, elongated along the direction perpendicular to the initial density gradient ∇n_0 [see Fig. 2(a)]. Since the scale–size along the direction perpendicular to ∇n_0 is nearly ten times larger than that along ∇n_0, Eq. (14) in Tanikawa *et al.* [6], which is obtained for a one–dimensional case, can give correct estimates for the eigenfrequencies of our caviton. If the observed depth and width of the caviton, $D \equiv |\delta n/n_c| \approx 0.6$ and $W \approx 1$ cm, are used, we obtain $f_{\ell=0} = \omega_1/2\pi \approx 1.79\times10^9$ Hz and $\Delta/2\pi = f_0 - 2f_{\ell=0} \approx -7.6 \times 10^8$ Hz. Using Eq. (18) with these values leads to the threshold field strength of the pump EPW at ω_0 for the degenerate parametric decay process in the caviton as $|\tilde{E}_0|_{\rm th} \approx 9.6$ kV/cm. Here, we have neglected the second term in the right–hand side of Eq. (18) since $\nu_1/\Delta < 0.01$ in our case.

Next, we have attempted to experimentally estimate the field strength of the EPW at ω_0 at the caviton using an electrostatically insulated rf pick-up probe which was calibrated using an electron–beam diagnostic technique [6, 7]. The maximum field strength of $|\tilde{E}_0| \approx 12.6$ kV/cm at the input microwave power of $P_{\rm in} \approx 100$ kW was obtained. This experimentally estimated field strength of the EPW at ω_0 at the caviton is about 30% above the theoretically estimated threshold field strength of the EPW at ω_0 for the degenerate parametric instability process in the caviton.

The growth time γ^{-1} for the $(1/2)\omega_0$ electron oscillations estimated using Eq. (16) is less than 10 ns which is much faster than the temporal resolution of our detection system (≥ 50 ns).

The broadened spectrum feature of the $(1/2)\omega_0$ electron oscillations observed in Fig. 6(a) can be understood if we take into account the effect of the non-degenerate processes. Equation (15) suggests that the frequency spectrum of the $(1/2)\omega_0$ electron oscillations os broadened around the frequency $(1/2)\omega_0$ by $\pm(1/2)|\omega_1 - \omega_2|$, where ω_1 and ω_2 are the eigenfrequencies of the $\ell = 0$ and $\ell = 1$ caviton eigenmodes, respectively. Using Eq. (15) with $f_{\ell=0} \approx 1.79 \times 10^9$ Hz and $f_{\ell=1} \approx 1.83 \times 10^9$ Hz for our caviton, we obtain

$$\mathrm{Re}\,\frac{\omega}{2\pi} = \frac{1}{2}f_0 \pm \frac{1}{2}|f_{\ell=0} - f_{\ell=1}| = \frac{1}{2}f_0 \pm 20 \ \text{MHz} . \qquad (19)$$

This agrees well with the experimental observation that the spectrum of $(1/2)\omega_0$ electron oscillations is broadened by approximately ± 15 MHz around $(1/2)f_0$.

5. EMISSION OF $(3/2)\omega_0$ ELECTROMAGNETIC WAVES FROM CAVITONS

In this section, we estimate the radiation power of $(3/2)\omega_0$ em waves from cavitons.

Although electron oscillations in the caviton are electrostatic in nature, the localized structure of the caviton provides the transverse component in the current which contributes to the $(3/2)\omega_0$ em radiation. To make the calculation simple, we assume the caviton as a localized current source acting as an antenna embedded in a vacuum.

The nonlinear current oscillating at $(3/2)\omega_0$ is produced in the caviton due to the beating between the oscillating electric field associated with the pump EPW at ω_0 and the parametrically enhanced $(1/2)\omega_0$ electron oscillations. This current can be expressed as

$$\mathbf{j}_{3/2} = -e(n_0\mathbf{V}_{1/2} + n_{1/2}\mathbf{V}_0), \tag{20}$$

where $n_0 = -(1/4\pi e)\nabla\cdot\mathbf{E}_0$, $n_{1/2} = -(1/4\pi e)\nabla\cdot\mathbf{E}_{1/2}$, $\mathbf{V}_0 = e\mathbf{E}_0/\mathrm{Im}\omega_0$, $\mathbf{V}_{1/2} = 2e\mathbf{E}_{1/2}/\mathrm{Im}\omega_0$, and $\mathbf{E}_0$ and $\mathbf{E}_{1/2}$ are the high-frequency electric fields associated with the pump EPW at ω_0 and the parametrically enhanced electron oscillations at $(1/2)\omega_0$, respectively.

The vector potential for radiation fields due to the localized $(3/2)\omega_0$ current is given by [13] (Ch.9)

$$\mathbf{A}_{3/2}(\mathbf{R},t) = \frac{1}{c}\int_V \mathrm{d}^3\mathbf{r}\int \mathrm{d}t'\,\frac{\mathbf{j}_{3/2}(\mathbf{r},t')}{|\mathbf{R}-\mathbf{r}|}\,\delta\left(t' + \frac{|\mathbf{R}-\mathbf{r}|}{c} - t\right), \tag{21}$$

where the vector $\mathbf{R}$ specifies the observation point, $\mathbf{r}$ is the position vector in the source region, and the volume integral is taken over the volume of the caviton, *i.e.*, the volume that contains the source current.

Assuming the sinusoidal time-dependencies for $\mathbf{j}_{3/2}$ and consequently for $\mathbf{A}_{3/2}$:

$$\mathbf{j}_{3/2}(\mathbf{r},t) = \mathbf{j}_{3/2}(\mathbf{r})\exp[-(3/2)\omega_0 t], \tag{22a}$$

$$\mathbf{A}_{3/2}(\mathbf{r},t) = \mathbf{A}_{3/2}(\mathbf{r})\exp[-(3/2)\omega_0 t], \tag{22b}$$

we obtain

$$\mathbf{A}_{3/2}(\mathbf{R}) = \frac{1}{c}\int_V \mathbf{j}_{3/2}(\mathbf{r})\frac{\exp(ik_{3/2}|\mathbf{R}-\mathbf{r}|)}{|\mathbf{R}-\mathbf{r}|}\,\mathrm{d}^3\mathbf{r}, \tag{23}$$

where $k_{3/2} = |\mathbf{k}_{3/2}|$ is the magnitude of the wavenumber of the $(3/2)\omega_0$ em wave.

In a far-field approximation ($k_{3/2}\mathrm{R} \to \infty$, where $\mathrm{R} = |\mathbf{R}|$), Eq. (23) can be reduced to

$$\mathbf{A}_{3/2}(\mathbf{R}) \simeq \frac{\exp(ik_{3/2}\mathrm{R})}{c\mathrm{R}}\int_V \mathbf{j}_{3/2}(\mathbf{r})\exp(ik_{3/2}\cdot\mathbf{r})\,\mathrm{d}^3\mathbf{r}. \tag{24}$$

Assuming the caviton is pancake–shaped (see Fig. 7), we approximate the spatial distribution of the $(3/2)\omega_0$ current using Gaussian form factors. For simplicity, the direction of $\mathbf{j}_{3/2}$ is set to be along the z-axis, *i.e.*, the initial density gradient ∇n_0. Then, the $(3/2)\omega_0$ current can be given by the following expression:

$$\mathbf{j}_{3/2}(\mathbf{r}) \simeq \hat{e}_z \frac{3}{4\pi} \frac{e}{m\omega_0} \frac{1}{W} \tilde{\mathbf{E}}_0 \tilde{\mathbf{E}}_{1/2} \exp(-\rho^2/\mathbf{R}_0^2) \exp(-4z^2/W^2), \quad (25)$$

where $\hat{e}_z$ is the unit vector along the z-axis, $\mathbf{R}_0$ is the radial scale–length of the pancake–shaped caviton, and $\mathbf{E}_0$ and $\mathbf{E}_{1/2}$ are represented by their peak values $\tilde{\mathbf{E}}_0$ and $\tilde{\mathbf{E}}_{1/2}$, respectively. Substituting Eq. (25) into Eq. (24), we obtain

$$\mathbf{A}_{3/2}(\mathbf{R}) \simeq \frac{\exp(ik_{3/2}\mathbf{R})}{c\mathbf{R}} \hat{e}_z F(\theta), \quad (26)$$

where

$$F(\theta) \equiv \frac{3}{8}\pi^{1/2} \frac{e}{m\omega_0} R_0^2 \tilde{E}_0 \tilde{E}_{1/2} G(\theta) \quad (27)$$

and

$$G(\theta) \equiv \exp[-(1/4)R_0^2 k_{3/2}^2 \sin^2\theta - (1/16)W^2 k_{3/2}^2 \cos^2\theta]. \quad (28)$$

The relationship between the various variables used in the calculation is depicted schematically in Fig. 7.

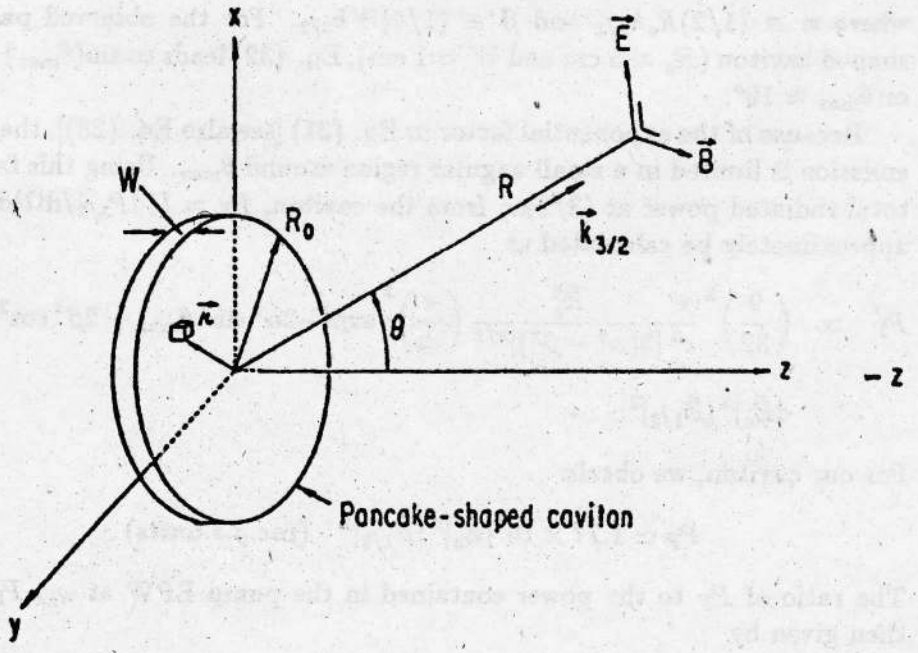

Fig.7. Geometry for the calculation of the radiated power of the em waves at $(3/2)\omega_0$ emitted by a pancake–shaped caviton.

The vector potential given by Eq. (26) is used to calculate the fields associated with the $(3/2)\omega_0$ radiation as follows:

$$\mathbf{B}_{3/2} = \nabla \times \mathbf{A}_{3/2}, \tag{29a}$$

$$\mathbf{E}_{3/2} = (i/k_{3/2})\nabla \times \mathbf{B}_{3/2}, \tag{29b}$$

where the relation $(3/2)\omega_0 = ck_{3/2}$ has been used. The time-averaged power radiated per unit solid angle by the oscillating current $\mathbf{j}_{3/2}$ is then given by

$$\frac{dP_{3/2}}{d\Omega} = \frac{c}{8\pi}\mathrm{Re}\langle R^2\hat{n}\cdot(\mathbf{E}_{3/2}\times\mathbf{B}^*_{3/2})\rangle, \tag{30}$$

where

$$\hat{n} \equiv k_{3/2}/|k_{3/2}|.$$

Using Eqs. (26)–(30), the angular distribution of radiated power at $(3/2)\omega_0$ can be obtained as

$$\frac{dP_{3/2}}{d\Omega} = \frac{9}{32\pi}\frac{\omega_0^2}{c^3}\sin^2\theta|F(\theta)|^2. \tag{31}$$

From this equation, the angle at which the radiated power is the maximum, $\theta_{\max}$, can be easily calculated as

$$\theta_{\max} = \sin^{-1}\left(\frac{1}{[2(\alpha^2-\beta^2)]^{1/2}}\right), \tag{32}$$

where $\alpha \equiv (1/2)R_0k_{3/2}$ and $\beta \equiv (1/4)Wk_{3/2}$. For the observed pancake-shaped caviton ($R_0 \approx 5$ cm and $W \approx 1$ cm), Eq. (32) leads to $\sin(\theta_{\max}) \approx 0.32$ or $\theta_{\max} \approx 19^\circ$.

Because of the exponential factor in Eq. (31) [see also Eq. (28)], the strong emission is limited in a small angular region around $\theta_{\max}$. Using this fact, the total radiated power at $(3/2)\omega_0$ from the caviton, $P_T = \int(dP_{3/2}/d\Omega)d\Omega$, can approximately be calculated as

$$P_T \simeq \left(\frac{9}{32}\right)^2\frac{\pi}{c^3}\frac{R_0^4}{[2(\alpha^2-\beta^2)]^{3/2}}\left(\frac{e}{m}\right)^2\exp(-2\alpha^2\sin^2\theta_{\max}-2\beta^2\cos^2\theta_{\max})\cdot$$
$$\cdot|\dot{\tilde{E}}_0|^2|\tilde{E}_{1/2}|^2. \tag{33}$$

For our caviton, we obtain

$$P_T \simeq 1.77\times10^4|\dot{\tilde{E}}_0|^2|\tilde{E}_{1/2}|^2 \quad (inc.g.s.units). \tag{34}$$

The ratio of P_T to the power contained in the pump EPW at ω_0, P_{EPW}, is then given by

$$\frac{P_T}{P_{\mathrm{EPW}}} \simeq 5.66\times10^3\tau|\tilde{E}_{1/2}|^2 \quad (inc.g.s.units), \tag{35}$$

where τ is the duration of the $(3/2)\omega_0$ radiation burst.

The saturation level of the non-resonant oscillations at $(1/2)\omega_0$ can be determined by the relation [14],

$$e\phi_{1/2} \sim T_e, \tag{36}$$

where $\phi_{1/2}$ is the potential associated with the $(1/2)\omega_0$ electron oscillations. Since $E_{1/2} \sim \phi_{1/2}/W$, we obtain

$$\frac{|\tilde{E}_{(1/2)\text{sat}}|^2}{8\pi n_B T_e} \sim \left(\frac{\lambda_D}{W}\right)^2, \tag{37}$$

where n_B is the plasma density at the bottom of the caviton and λ_D should be evaluated at the same position. Using this relation, we obtain that $|\tilde{E}_{(1/2)\text{sat}}|$ is of the order of 1 V/cm for our case. Adopting this level of $|\tilde{E}_{(1/2)\text{sat}}|$ and the typical duration of the radiation burst, $\tau \approx 0.13$ μs, Eq. (35) gives $P_T/P_{\text{EPW}} \approx -81$ dB. If we take into account the following two factors: 1) the resonance absorption fraction of the incident microwave estimated using the effective microwave incident-angle of $\sim 20^\circ$ inferred from the wave propagation measurements to be $\sim 20\%$, and 2) the $(3/2)\omega_0$ radiation power collected by the horn detector estimated from the antenna pattern to be $\sim 10\%$ of the total radiated power, we can estimate the ratio of the $(3/2)\omega_0$ radiation power collected by the horn detector to the incident microwave power as

$$\frac{P_{(3/2)\text{collected}}}{P_{\text{in}}} \approx -98 \text{ dB}. \tag{38}$$

This value agrees well with the experimentally determined $P_{(3/2)\text{collected}}/P_{\text{in}} \approx \approx -100$ dB (see Fig. 5).

According to Eq. (20), we should expect that the frequency spectrum of $(3/2)\omega_0$ radiation is identical to that of $(1/2)\omega_0$ electron oscillations. The simple theory presented in this section cannot explain the different features between the two different frequency spectra (see Fig. 6). However, we note that the frequency spectrum of $(3/2)\omega_0$ radiation was measured after the $(3/2)\omega_0$ em waves had propagated through the turbulent plasma region. This might have altered the dispersion relation for the $(3/2)\omega_0$ em waves, resulting in the frequency splitting feature observed in the frequency spectrum of $(3/2)\omega_0$ radiation [15].

6. CONCLUSIONS

We have experimentally identified a new generation mechanism for $(3/2)\omega_0$ em radiation from an inhomogeneous plasma under intense em irradiation. This mechanism involves the generation of deep ($|\delta n/n_c| \geq 0.5$) density cavities at the critical layer. A resonantly excited EPW at the critical layer upon

the injection of the intense microwave pulse digs a deep density cavity by its ponderomotive force. The wave intensity increases as the wave is trapped in the cavity (the formation of a caviton). Subsequently, the trapped wave undergoes a parametric decay process to enhance the non-resonant electron oscillations at frequency $(1/2)\omega_0$ in the caviton once the wave intensity exceeds a certain critical value determined by the depth and shape of the caviton. The localized, nonlinear current oscillating at $(3/2)\omega_0$ due to the beating of the trapped EPW at ω_0 and the $(1/2)\omega_0$ electron oscillations causes the emission of em waves at $(3/2)\omega_0$ from the caviton.

A simple theory to describe the above processes has been developed. The theory predicts that the field strength of the trapped EPW at ω_0 should exceed ~ 9.6 kV/cm for the generation of $(3/2)\omega_0$ radiation from the observed pancake-shaped caviton. Our observations have shown that this threshold field strength is always surpassed under our experimental conditions. The radiated power at $(3/2)\omega_0$ from the caviton predicted by our theory agrees well with the experimental observation. However, our theory cannot explain the different features between the frequency spectrum of $(3/2)\omega_0$ radiation and that of $(1/2)\omega_0$ electron oscillations. The physical model to explain the generation of $(3/2)\omega_0$ radiation is summarized in Fig. 8. This phenomenon associated with the appearance of very deep cavitons in a rather short time-scale may be related to the collapsing of cavitons [16].

It is hoped that our new discovery can help us understand some of the puzzling effects associated with subharmonic emissions in ionospheric modification and laser-plasma interaction experiments. Finally, it is pointed out that the detection of em radiation at $(3/2)\omega_0$ emitted by cavitons can be used as a remote diagnostic means to estimate the strength of localized EPWs and the depth of associated density cavities.

ACKNOWLEDGMENTS

The work performed at UCLA was supported by the US National Science Foundation. This work was also partially supported by A Grant-in-Aid for Scientific Research: International Scientific Program-Joint Research of the Ministry of Education, Science and Culture, Japan.

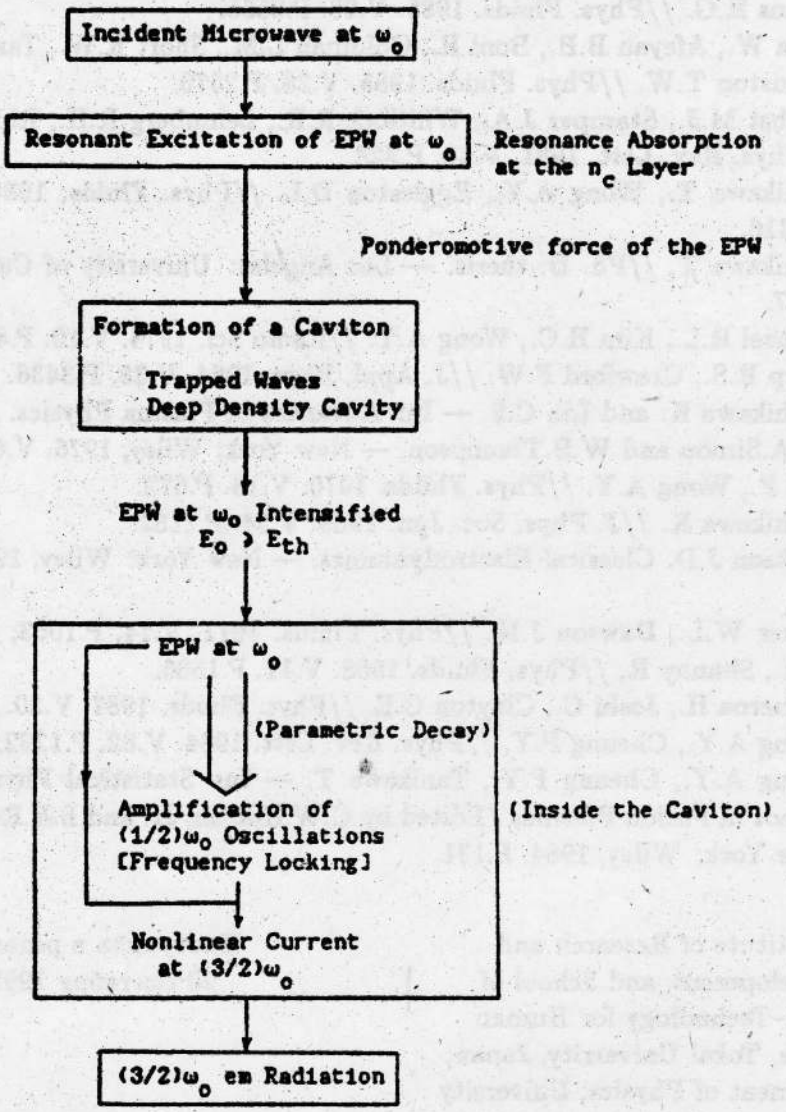

Fig.8. Physical model for the generation of $(3/2)\omega_0$ em radiation from a caviton.

REFERENCES

1. Derblom H., Thidé B., Leyser T.B., Nordling J.A., Hedberg A., Stubbe P., Kopka H., Rietveld M. //J. Geophys. Res. 1989. V.94(A8). P.10,111.
2. Avrov A.I., Bychenkov V.Yu., Krokhin O.N., Pustovalov V.V., Rupasov A.A., Silin V.P., Sklizkov G.V., Tikhonchuk V.T., Shikanov A.S. //Zh. Eksp. Teor. Fiz. 1977. V.72. P.970; [//Sov. Phys. JETP. 1977. V.45. P.507].

3. Aboites V., Hughes T.P., McGoldrick E., Sim S.M.L., Karttunen S.J., Evans R.G. //Phys. Fluids. 1985. V.28. P.2555.
4. Seka W., Afeyan B.B., Boni R., Goldman L.M., Short R.W., Tanaka K., Johnston T.W. //Phys. Fluids. 1985. V.28. P.2570.
5. Herbst M.J., Stamper J.A., Whitlock R.R., Lehmberg R.H., Ripin B.H. //Phys. Rev. Lett. 1981. V.46. P.328.
6. Tanikawa T., Wong A.Y., Eggleston D.L. //Phys. Fluids. 1984. V.27. P.1416.
7. Tanikawa T. //Ph. D. thesis. — Los Angeles: University of California, 1987.
8. Stenzel R.L., Kim H.C., Wong A.Y. //Radio Sci. 1974. V.10. P.485.
9. Harp R.S., Crawford F.W. //J. Appl. Phys. 1964. V.35. P.3436.
10. Nishikawa K. and Liu C.S. — In: Advances in Plasma Physics. /Edited by A.Simon and W.B.Thompson. — New York: Wiley, 1976. V.6. P.3.
11. Hai F., Wong A.Y. //Phys. Fluids. 1970. V.13. P.672.
12. Nishikawa K. //J. Phys. Soc. Jpn. 1968. V.24. P.1152.
13. Jackson J.D. Classical Electrodynamics. — New York: Wiley, 1975, 2nd ed.
14. Kruer W.L., Dawson J.M. //Phys. Fluids. 1971. V.14. P.1003; Dawson J.M., Shanny R. //Phys. Fluids. 1968. V.11. P.1506.
15. Figueroa H., Joshi C., Clayton C.E. //Phys. Fluids. 1987. V.30. P.586.
16. Wong A.Y., Cheung P.Y. //Phys. Rev. Lett. 1984. V.52. P.1222; Wong A.Y., Cheung P.Y., Tanikawa T. — In: Statistical Physics and Chaos in Fusion Plasmas /Edited by C.W.Horton, Jr. and L.E.Reichl. — New York: Wiley, 1984. P.131.

Institute of Research and Development, and School of High–Technology for Human Welfare, Tokai University, Japan; Department of Physics, University of California, Los Angeles, U.S.A.

Поступила в редакцию
20 сентября 1993 г.